UNCONSTRAINED HETEROGENEOUS COLLOIDAL QUANTUM DOTS EMBEDDED IN GaAs/GaSb NANOVOIDS

Marek Osinski and Ganesh Balakrishnan

University of New Mexico
Center for High Technology Materials
1313 Goddard SE
Albuquerque, NM 87106-4343

17 Apr 2014

Final Report

AIR FORCE RESEARCH LABORATORY
Space Vehicles Directorate
3550 Aberdeen Ave SE
AIR FORCE MATERIEL COMMAND
KIRTLAND AIR FORCE BASE, NM 87117-5776

DTIC COPY
NOTICE AND SIGNATURE PAGE

This report is the result of contracted fundamental research deemed exempt from public affairs security and policy review in accordance with SAF/AQR memorandum dated 10 Dec 08 and AFRL/CA policy clarification memorandum dated 16 Jan 09. This report is available to the general public, including foreign nationals. Copies may be obtained from the Defense Technical Information Center (DTIC) (http://www.dtic.mil).

AFRL-RV-PS-TR-2014-0003 HAS BEEN REVIEWED AND IS APPROVED FOR PUBLICATION IN ACCORDANCE WITH ASSIGNED DISTRIBUTION STATEMENT

//SIGNED//   //SIGNED//
CLAY MAYBERRY   JAMES LYKE
Program Manager   Tech Advisor, Space Electronics Protection Branch

//SIGNED//
BENJAMIN M. COOK, Lt Col, USAF
Deputy Chief, Spacecraft Technology Division
Space Vehicles Directorate

This report is published in the interest of scientific and technical information exchange, and its publication does not constitute the Government's approval or disapproval of its ideas or findings.

REPORT DOCUMENTATION PAGE

1. REPORT DATE *(DD-MM-YYYY)* 17-04-2014	2. REPORT TYPE Final Report	3. DATES COVERED *(From - To)* 30 Nov 2012 – 28 Feb 2014

4. TITLE AND SUBTITLE Unconstrained Heterogeneous Colloidal Quantum Dots Embedded in GaAs/GaSb Nanovoids	
	5a. CONTRACT NUMBER
	5b. GRANT NUMBER FA9453-13-1-0221
	5c. PROGRAM ELEMENT NUMBER 62601F
6. AUTHOR(S) Marek Osinski and Ganesh Balakrishnan	5d. PROJECT NUMBER 4846
	5e. TASK NUMBER PPM00017819
	5f. WORK UNIT NUMBER EF009789

7. PERFORMING ORGANIZATION NAME(S) AND ADDRESS(ES) University of New Mexico Center for High Technology Materials 1313 Goddard SE Albuquerque, NM 87106-4343	8. PERFORMING ORGANIZATION REPORT NUMBER
9. SPONSORING / MONITORING AGENCY NAME(S) AND ADDRESS(ES) Air Force Research Laboratory Space Vehicles Directorate 3550 Aberdeen Ave., SE Kirtland AFB, NM 87117-5776	10. SPONSOR/MONITOR'S ACRONYM(S) AFRL/RVSE
	11. SPONSOR/MONITOR'S REPORT NUMBER(S) AFRL-RV-PS-TR-2014-0003

12. DISTRIBUTION / AVAILABILITY STATEMENT

Approved for public release; distribution is unlimited.

13. SUPPLEMENTARY NOTES

14. ABSTRACT
The objective of this project was to create a novel template of nanovoids that could then be used for integration of a variety of colloidal quantum dots (CQDs) with a III-V matrix. More specifically, the project dealt with the issues related to the creation of *in situ* nanovoids, the development of sites in these nanovoids for attachment of the CQDs, and finally the ability to encapsulate the CQDs in the III-V matrix. An innovative and novel approach for the fabrication of the nanovoids was demonstrated, using a molecular-beam-epitaxy (MBE)-based *in situ* etching process that enabled the creation of the nanovoids on a GaSb epilayer using an As flux, thus eliminating the need for post-growth wet or dry etching processes. The As-based etching resulted in crystallographically faceted nanovoids, which are unique to this process. It should be noted that due to surface tension, wet-etching techniques cannot form nanovoids on this scale, while dry etching techniques cannot create faceted voids critical for anchoring CQDs. This project represents a completely novel approach towards the integration of non-epitaxially grown CQDs with MBE-based epitaxial structures, and its successful completion enables the realization of an entirely new class of heterogeneous devices.

15. SUBJECT TERMS
Heterogeneous Integration; Colloidal Quantum Dots; Nanovoids; GaSb; GaAs

16. SECURITY CLASSIFICATION OF:			17. LIMITATION OF ABSTRACT	18. NUMBER OF PAGES	19a. NAME OF RESPONSIBLE PERSON Clay Mayberry
a. REPORT Unclassified	b. ABSTRACT Unclassified	c. THIS PAGE Unclassified	Unlimited	40	19b. TELEPHONE NUMBER *(include area code)*

This Page Left Intentionally Blank

TABLE OF CONTENTS

LIST OF FIGURES AND TABLES

ACKNOWLEDGMENTS

DISCLAIMER

The views and conclusions contained herein are those of the authors and should not be interpreted as necessarily representing the official policies or endorsements, either expressed or implied, of Air Force Research Laboratory or the U.S. Government.

(This page intentionally left blank)

1.0   SUMMARY

The objective of this project was to create a novel template of nanovoids that could then be used for integration of a variety of colloidal quantum dots (CQDs) with a III-V matrix. More specifically, the project dealt with the issues related to the creation of *in situ* nanovoids, the development of sites in these nanovoids for attachment of the CQDs, and finally the ability to encapsulate the CQDs in the III-V matrix. An innovative and novel approach for the fabrication of the nanovoids was demonstrated, using a molecular-beam-epitaxy (MBE)-based *in situ* etching process that enabled the creation of the nanovoids on a GaSb epilayer using an As flux, thus eliminating the need for post-growth wet or dry etching processes. The As-based etching resulted in crystallographically faceted nanovoids, which are unique to this process. It should be noted that due to surface tension, wet-etching techniques cannot form nanovoids on this scale, while dry etching techniques cannot create faceted voids critical for anchoring CQDs. This project represents a completely novel approach towards the integration of non-epitaxially grown CQDs with MBE-based epitaxial structures, and its successful completion enables the realization of an entirely new class of heterogeneous devices.

2.0   INTRODUCTION

The process of etching is extremely important and well established for various stages of fabrication of semiconductor devices. While most etching processes are *ex-situ* and involve the removal of several micrometers of materials to delineate one or more layers of the semiconductor for applications that range from metallization to regrowth, more novel etching applications are *in-situ* and on a nanoscale. Applications for these nanoscale etching processes include nanochannel formation, delineation of nanospaces for insertion of CQDs, and flash-memory device fabrication. Etching on a nanoscale is presently achieved through e-beam lithography, scanning-tunneling-microscopy-assisted lithography, optical lithography, and *in-situ* processes such as bromine-based MBE etching of III-As compounds. The *in-situ* etching techniques have a distinct advantage over the *ex-situ* techniques when it comes to both CQD integration as well as regrowth, since the surface is free of contaminants and native oxides.

3.0   METHODS, ASSUMPTIONS, AND PROCEDURES

3.1   Experimental Details of MBE Growth

The samples were grown in a V80H MBE reactor. Valve crackers were used as the As and the Sb sources. Operating temperatures were 900 °C and 950 °C, resulting in As_2 and Sb_2, respectively. A pyrometer was used to measure the temperature of the substrate and a reflective high-energy electron beam (RHEED) system in conjunction with a KSA™ RHEED analysis was used to monitor the growth surface. The growth was started on a GaSb substrate through a thermal oxide desorption process at 540 °C and then a GaSb smoothing layer at 510 °C was grown. A III:V beam equivalent pressure (BEP) ratio of 1:6 was used to grow GaSb. The RHEED pattern was used to check for a (3×1) pattern, as this indicated that the GaSb grown was extremely smooth. Next, the growth was stopped to allow excess Sb to be desorbed from the GaSb surface. Then, the surface was exposed to an As_2 overpressure, with the substrate at 510 °C. This exposure of the surface to As_2 altered the RHEED from a (3×1) to an unidentifiable

1

"murky" pattern. After a 60 s As_2 soak, the remnants of the (3×1) reconstructions were no longer present. The GaAs growth was then initiated. The growth temperature was kept constant at 510 °C. This resulted in a smoothing of the surface, with continued growth for about 20 nm. A III:V BEP ratio of 1:10 was used for the GaAs growth.

3.2 Formation of Nanovoids

Nanopits can be etched *in-situ* on GaSb substrate using an atomic flux of cracked arsenic (As_2) as an etchant. GaSb acts as a membrane material for making the nanopores. This process, therefore, aids GaSb *in- situ etching* without requiring any complex equipment modifications. Subsequent GaAs overgrowth continues by coalescence over the etched pits, forming nanovoids at the GaAs/GaSb interface. This is, then, followed by planar growth of the bulk material. The highly faceted feature of the nanovoids may also allow encapsulation schemes for the development of novel quantum-confined ensembles [1], [2]. The nanoscale dimensions of the voids would exhibit quantum-size effects for the encapsulated material. This process is extremely successful, as the etch rate can be controlled using both the substrate temperature as well as the arsenic species. Moving from As_4 to As_2 to As, the etching becomes more aggressive. Which of these species is generated can be controlled easily by changing the valved cracker's cracking zone temperature.

GaSb reacts with As_2 due to a negative enthalpy of reaction, as described by Losurdo *et al*. [3]. The As_2 specie reacts strongly with GaSb for both 1) the anion exchange reaction and 2) the isoelectronic AsSb compound formation reaction, where

$$2GaSb + As_2 \rightarrow 2GaAs + Sb_2 \ , \qquad \Delta H = -47.6 \ \text{kJ/mol, and} \tag{1}$$

$$GaSb + As_2 \rightarrow GaAs + AsSb \ , \qquad \Delta H = -33.9 \ \text{kJ/mol,} \tag{2}$$
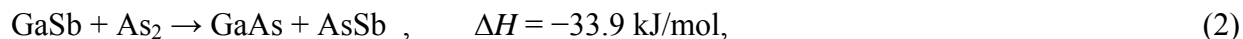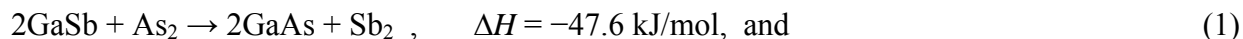
where ΔH is a change in enthalpy caused by the reaction. It is observed that in both reactions, the As_2 gas aggressively reacts with GaSb to form GaAs and either excess Sb [Eq. (1)] or AsSb [Eq. (2)]. Based on the above reactions, it has been established that GaSb surfaces can be etched by As_2 and the etch process causes formation of faceted pits, a process that is comparable to other etching processes [4]-[6].

3.3 Electron Microscopy

The As_2-induced etched pits on the GaSb surface were analyzed using a Hitachi S-5200 scanning electron microscope (SEM), illustrated in Figure 1. The Hitachi S-5200 Nano SEM at the University of New Mexico is one of the highest resolution SEMs available today. The microscope has a magnification range from 100 to 2,000,000, with guaranteed resolution of 1.7 nm at 1 kV and 0.5 nm at 30 kV. It is equipped with both secondary and backscatter electron detectors.

Approved for public release; distribution is unlimited.

Figure 1. The Hitachi S-5200 Nano SEM at the University of New Mexico

3.4   Synthesis of CdSe/ZnS Core/Shell Colloidal Quantum Dots

The term "colloidal" refers to a colloidal dispersion, which is a heterogeneous mixture that visually appears to be a homogeneous solution. It is a mixture of two material phases, in our case solid-phase nanoparticles dispersed in a homogeneous liquid phase. The nanoparticles that are distributed evenly throughout the continuous liquid phase are held in a dynamically stable state supported by two equal but opposing forces: the van der Walls force of attraction and the electrostatic repulsion. The inorganic cores of CQDs exhibit useful properties controlled by composition as well as size and shape, while the organic surfactant coating ensures stability. It is this combination that makes CQDs attractive and promising for novel applications.

The synthesis of CQDs occurs in three stages, namely nucleation, growth, and Ostwald ripening. These stages are controlled by some key factors, such as concentration and chemistry of reagents and surfactants, temperature, growth time, and surfactant to reagent ratio. Monodisperse CQDs can be obtained by rapid injections of reagents into a reaction vessel containing a hot, coordinating solvent. This high temperature solvent decomposes the reagents, forming a supersaturation of molecules in solution, which leads to the concentration dropping below the critical concentration and hence nucleation of the QDs. A uniform surface regularity in core structure can be achieved through slow growth and annealing of the QDs in the coordinating solvent.

3

For synthesis of CQDs using wet chemical bottom-up approach, the entire reaction needs to be conducted in an inert atmosphere, which enables handling of air-sensitive precursors, reduces the danger of contamination and/or oxidation of the produced CQDs, and also provides for the removal of any gas byproducts from the reaction. For this purpose, a specialized laboratory glassware system known as Schlenk line is used, which provides a controlled pressure, and pure argon/nitrogen (inert) atmosphere for the reaction.

The reaction takes place in a three-neck round-bottom flask, with the center neck connected to one of the lines on the Schlenk line. The other two necks are sealed using rubber septa, with one septum used for inserting a thermocouple. The thermocouple is in turn connected to a ramping temperature controller. For continuous stirring of the solution in the flask, the flask contains a small cylindrical teflon-coated stir bar, which is spun using a rotating magnetic field generated by a stirring controller placed beneath the heating mantle. The round-bottom flask is placed firmly on top of the heating mantle, ensuring a good thermal contact.

The procedure for colloidal synthesis of CdSe/ZnS core/shell CQDs was adapted from [7]. The CdSe core was prepared using cadmium acetylacetonate [Cd(acac)$_2$] and trioctyl phosphine selenide (TOPSe). The ZnS shell was synthesized using diethylzinc (ZnEt$_2$) and bis(trimethylsilyl) sulfide [(TMS)$_2$S] (also called hexamethyldisilathiane) as precursors. The synthesis was carried out under strictly air-free atmosphere using the Schlenk line setup, illustrated in Figure 2. Precursor solutions were prepared under Ar atmosphere in different three-neck flasks by connecting them to the Schlenk line gas manifold.
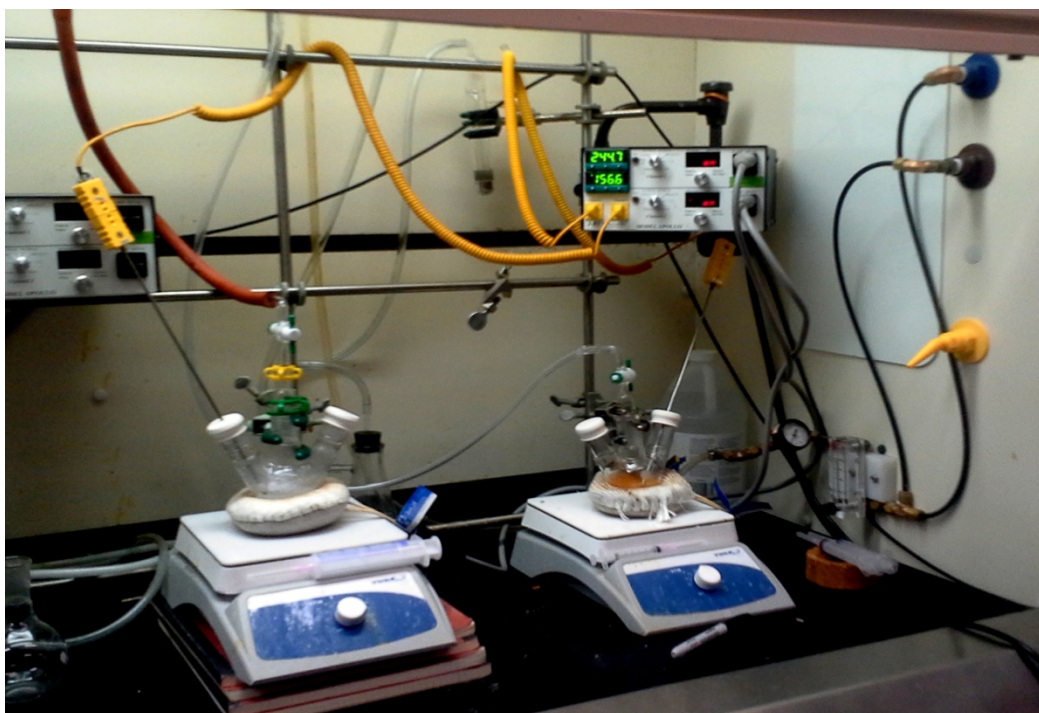
Figure 2. Schlenk Line Setup at the Center for High Technology Materials

First, 10 mL of trioctyl phosphine (TOP) and 0.79 g of selenium (Se) were mixed to create a 1 M stock solution of TOPSe in a 250 mL beaker. 20 g of trioctyl phosphine oxide (TOPO), 10 g of hexadecylamine (HDA), and 5 mL of TOP were added to a three-neck flask, which was then degassed in a vacuum and heated to 130 °C for 1.5 hours. Next, the Cd precursor was made by mixing 620 mg of $Cd(acac)_2$, 1.20 g of hexadecanediol (HDD), and 10 mL of TOP in a three-necked flask and heating it to 100 °C under vacuum, followed by cooling it to 80 °C. After that, 10 mL of the 1 M TOPSe stock solution was injected into the precursor. After 1.5 hours, the atmosphere was switched to argon and the temperature was raised to 340-350 °C. Under the ultraviolet (UV) light, 30 mL of Cd and Se precursors were injected rapidly into the hot solvent flask. The core of the CQDs was allowed to grow in this solution for about 3-4 minutes until it finished forming, as evidenced by a change in color to red under a UV lamp. As soon as the solution turned red, the temperature was lowered to 130 °C.

Next, the ZnS coating was synthesized. The temperature of the quantum dot (QD)/TOPO solution was decreased to 140-180 °C. 5 mL of TOP were then added to a beaker. After that, 2.69 mL of 1 M $ZnEt_2$ and sulfur precursor $[(TMS)_2S]$ were added to the TOP in the beaker. Then, 10 mL of the Zn and S precursor solution was very slowly added to the QD/TOPO solution and the temperature was lowered to 80 °C. The solution was stirred for several hours, followed by addition of equal amounts of butanol and hexane.

The resultant CQDs were harvested by centrifugation using methanol, after which a clear supernatant was observed. The supernatant was then discarded, leaving the CQDs as a precipitate. Finally, the CQDs were collected using hexane and stored in a glass vial. Figure 3 shows the synthesized CdSe/ZnS core/shell CQDs, emitting around 570 nm (greenish-yellow) light under a UV lamp illumination.
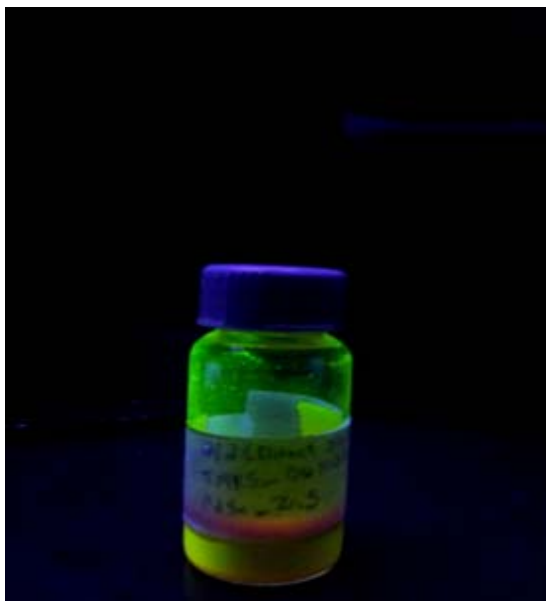
Figure 3. Synthesized CdSe/ZnS Core/Shell CQDs

3.5   Methodology of Temperature Sensitivity Testing of CdSe/ZnS Core/Shell CQDs

Before placing the CQDs in the nanovoids, we carried out some experiments to determine if the CQDs would still preserve their photoluminescence (PL) after being exposed to the high regrowth temperatures inside the MBE machine. In order to investigate this, we used silicon wafers with an etched depression as a holder to contain the CQDs. Steps involved were:

- identification of the type of silicon wafers
- identification of the right etchant
- determination of the etch process and time
- etch profile analysis using the Alpha-Step profilometer
- testing of thermal stability of the QDs via calcination (heating a substance to a high temperature, but below the melting or fusing point, causing loss of moisture, reduction or oxidation, and the decomposition of carbonates and other compounds) at the regrowth temperature of up to 700 °C.
- subjecting the wafer containing the QDs to a temperature of 480 °C in a vacuum environment
- measurements of the PL from the QDs prior to and after placing the QDs on the etched Si wafer

3.5.1   Identification of Silicon Wafers. Since the etchant and etch rate of a Si wafer depend on the orientation and doping of the wafer, it is important to determine the crystallographic orientation and doping type. By observing wafer flats, we can distinguish between silicon wafers of <100> and <111> orientation (Fig. 4) [8]. The purpose and function of wafer flats is the orientation for automatic equipment and to indicate type and orientation of crystal. There are two flats:

1. **Primary Flat:** The flat of longer length located in the circumference of the wafer. The primary flat indicates a specific crystalline orientation relative to the wafer surface.

2. **Secondary Flat:** The flat of shorter length located in the circumference of the wafer. This flat indicates the crystalline orientation and doping of the wafer. The location of this flat varies.

The standard convention for marking doping type and orientation of Si wafers is: 90° angle between the flats indicates a *p*-type <100> Si wafer [Fig. 4(a)]; 180° angle between the flats indicates an *n*-type <100> Si wafer [Fig. 4(b)]; absence of the secondary flat indicates a *p*-type <111> Si wafer [Fig. 4(c)]; and 45° angle between the flats indicates an *n*-type <111> Si wafer [9] [Fig. 4(d)].
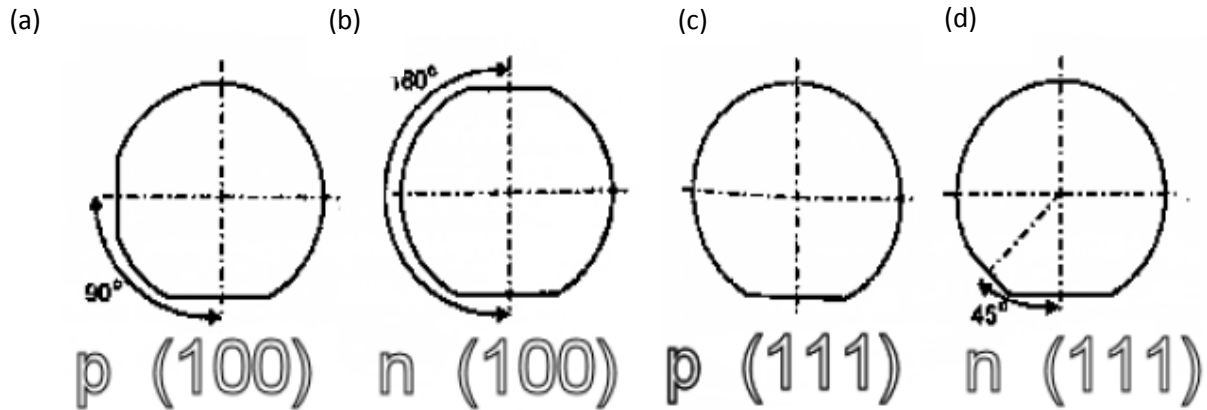
Figure 4. Standard Convention for Marking Doping Type and Orientation of Si Wafers

Using this guide, we have determined that the silicon wafers used in our experiments were of *p*-type and had the <100> orientation.

3.5.2   Anisotropic Silicon Etch Using Potassium Hydroxide Solution. Potassium hydroxide (KOH) is an etchant that attacks silicon preferentially in the <100> plane, producing a characteristic anisotropic V-etch with sidewalls that form a 54.7 ° angle with the surface (35.3 ° from the normal). This etch process is independent of the doping concentration for As, P, and Sb dopants. Table 1 shows the dependence of KOH etch rate on the temperature and Si-wafer orientation [9]. As with all wet-chemical etching solutions, the dissolution rate is a strong function of temperature. Significantly faster etch rates at higher temperatures are typical, but less ideal etch behavior is also common with more aggressive etch rates. Also, heavy boron doping can significantly harden the silicon and sharply reduce the etch rate [9].

7

Table 1: Temperature- and Silicon-Orientation-Dependent Etch Rates of KOH

Etchant	Temperature (°C)	Direction (plane)	Etch rate (μm min^{-1})	Remarks
20% KOH: 80% H$_2$O	20	(100)	0.025	Near Peak etch rate at the conc. across temperature
	40	(100)	0.188	
	60	(100)	0.45	
	80	(100)	1.4	
	100	(100)	4.1	
30% KOH: 70% H$_2$O	20	(100)	0.024	Smoother surfaces than at lower concentration
	40	(100)	0.108	
	60	(100)	0.41	
	80	(100)	1.3	
	100	(100)	3.8	
	20	(110)	0.035	
	40	(110)	0.16	
	60	(110)	0.62	
	80	(110)	2.0	
	100	(110)	5.8	
				Faster etch rate for (110) than for (100)

The following etching procedure was adopted:

- **Preparation of the etchant:** In order to prepare the 30% etchant, we used 70 g of KOH pellets and 190 ml of de-ionized (DI) water. We mixed the KOH pellets on a warm surface at about 80 °C until they completely dissolved. A stir-bar was placed into the beaker to ensure the mixing was done evenly [10].
- **Etching procedure:** First, we cleaned the wafer, using acetone, isopropyl alcohol (IPA), and DI water. The silicon wafer was placed in a beaker partially filled with acetone. Next, the beaker was placed in an ultrasonic bath (no heat) and the wafer was agitated (vibrated) for a few minutes. Tweezers were used to remove the wafer from the beaker. The wafer was, then, blown dry with nitrogen gas and the cleaning steps were consecutively repeated with IPA and DI water. While IPA and acetone helped to remove any organic contaminants from the wafer surface, DI water helped to wash off any ionic contaminants. Finally, the waste cleaning agents were disposed off into a waste container.

The cleaned wafer was placed in a Petri dish and heated to 80 °C in the oven. About 10 ml of the solution was taken in a pipette and a drop was placed on the hot wafer. The KOH bubbled at the exposed silicon sites while etching occurred. According to [9], the etch rate for 30% KOH

8

should be 1.3 µm/min, as shown in Table 1. Therefore, the wafer was left to etch for one minute, after which it was allowed to cool down. Finally, the wafer was cleaned once again, according to the procedure described above.

4.0   RESULTS AND DISCUSSION

4.1   Electron and Atomic Force Microscopy of Nanopits and Nanovoids

Figures 5(a) and 5(b) show plan-view and cross-sectional images of nanopits formed on the GaSb surface after exposure to As_2. The pit density in Figure 5(a) is $\sim 1 \times 10^9/cm^2$. The pits varied in both size and shape. The average dimensions were ~25 nm in width, 50–80 nm in length, and 10–70 nm in depth. There appears to be no significant directionality to the pit direction. The image in Figure 5(b) shows a (110)-cleaved facet with a 30 nm wide pit intercepted by the cleaving plane.

The resolution available using the high-resolution scanning electron microscope (HR-SEM) was not high enough to understand the faceting of the pits. However, a correlation was observed in the images of the pit structure from the surface and the cross-section, due to As_2 reaction with the GaSb substrate.

By grinding samples using mechanical methods to less than 10 µm of thickness and thinning the samples to electron transparency using an ion beam, specimens were prepared for high-resolution cross-sectional transmission electron microscope (XTEM). The atomic-force microscope (AFM) and XTEM images in Figures 6(a) and 6(b) reveal the faceted voids. They further reveal the progression of the GaAs overgrowth on the etched GaSb surface with the GaAs coverage increasing from 3 to 30 monolayers (MLs). Figure 6(a) shows the AFM image after a 10 Å (about 3 MLs) of GaAs deposition was done for 60 s. Surface remnants of the etched pits can be seen as dark features on the AFM image. This suggests that only a partial GaAs coalescence occurs over the pit after the 3-ML deposition has been carried out. The image shows a pit density of $1 \times 10^9/cm^2$, which is consistent with that observed in Figure 5(a). The lateral progression of GaAs overgrowth on the same sample is elucidated in the XTEM image of Figure 6(b). When the GaAs deposition is continued, the lateral overgrowth proceeds to coalesce over the pits, resulting in encapsulated nanovoids at the interface. It is further observed that no GaAs growth takes place inside the etched pits, thus creating the nanovoids.

9
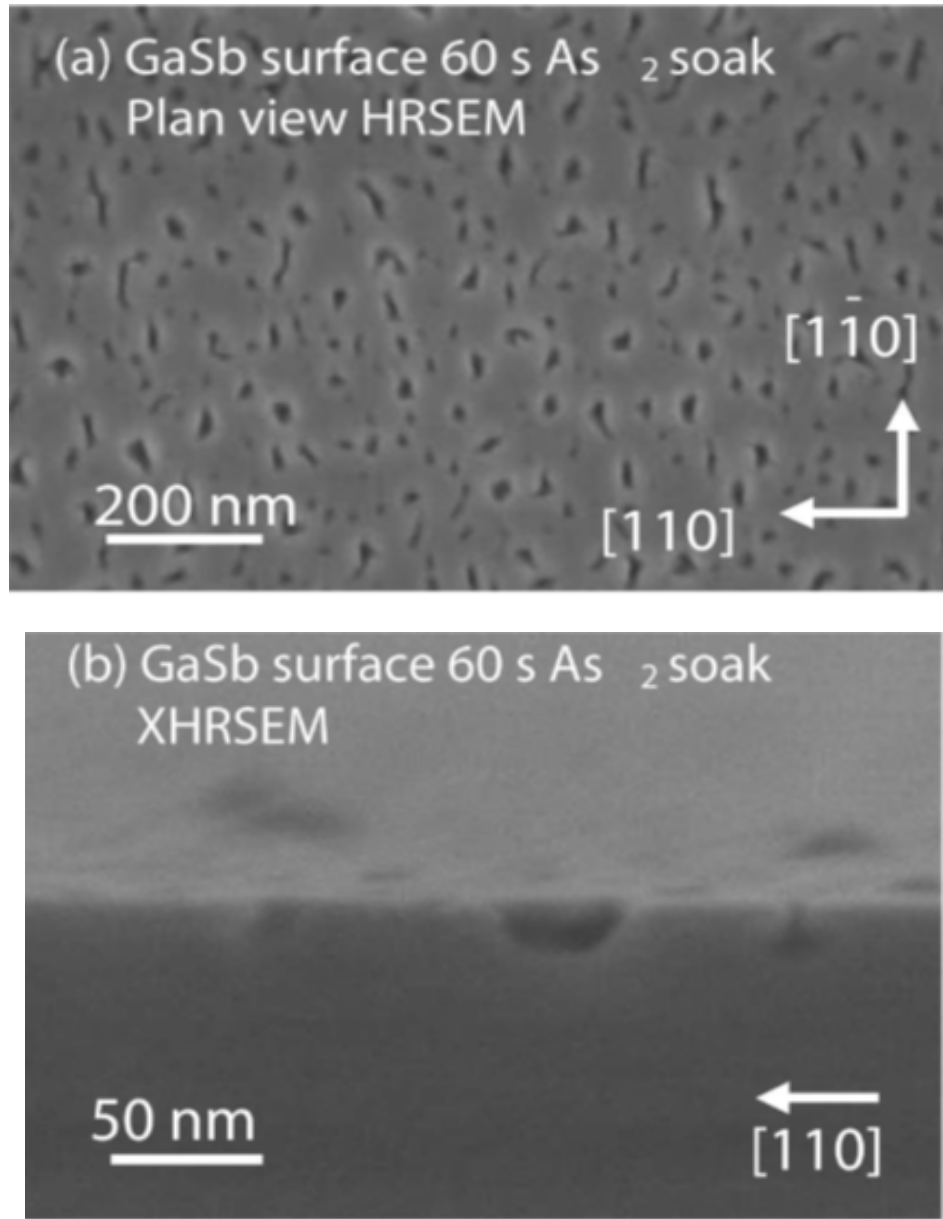
Figure 5. SEM Images of GaSb Surface After a 60-s Soak in As$_2$. (a) Plan View; (b) Side View

Figure 7 shows examples of nanovoids observed using XTEM [2]. The highly crystallographic nature of the etching results in a fixed triangular (V-shaped) contour of the nanovoids. Figure 7(a) shows a bright field (BF) transmission electron microscopy (TEM) analysis of V-shaped and truncated V-shaped nanovoids present on the GaAs/GaSb interface. The V-shaped nanovoid is enclosed by (111) and (1$\underline{11}$) sidewalls, while the truncated V-shaped nanovoid is also enclosed by (111) and (1$\underline{11}$) sidewalls, but is bounded at the bottom by a (100) plane.

10
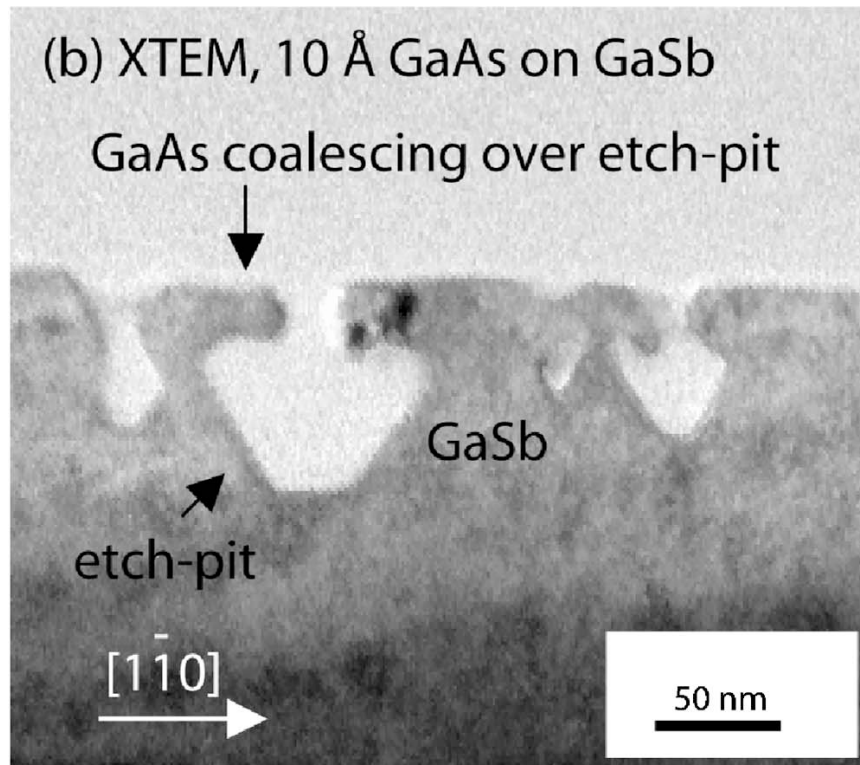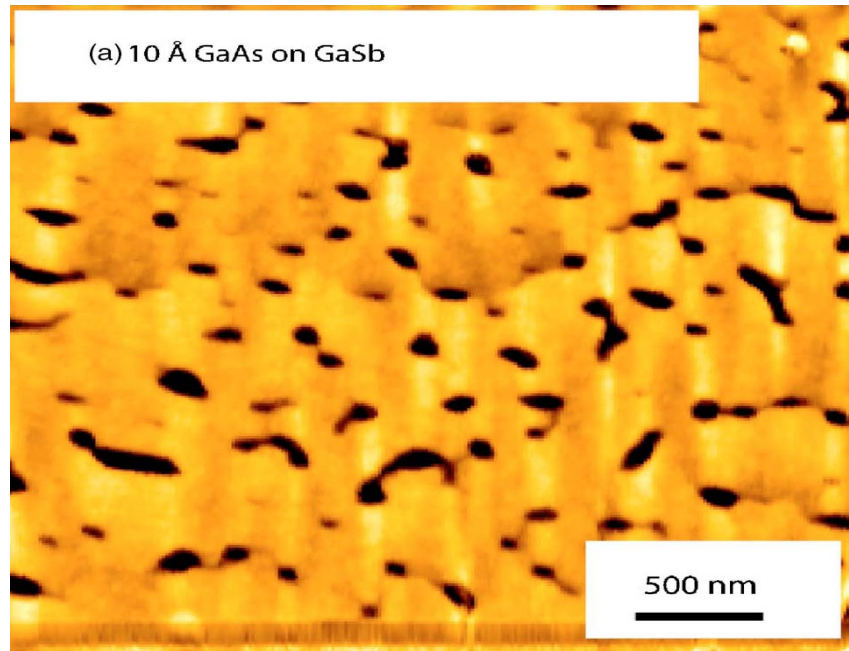
**Figure 6. (a) AFM Image of GaAs (10 Å) Overgrowth on GaSb Surface,
(b) XTEM Image Showing Partial GaAs Coalescence Over Etched Pits**

11

(a) BF, GaAs on GaSb

GaAs

voids

GaSb

50nm

[001]

[110]

(b) DF, v-shaped nanovoid

(110)

(111)

[001]

[110]

(111)

(110)

GaAs

GaSb

100 nm

(c) DF, truncated nanovoid

(110)

(111)

[001]

[110]

(100)

(111)

(110)

GaAs

GaSb

100 nm
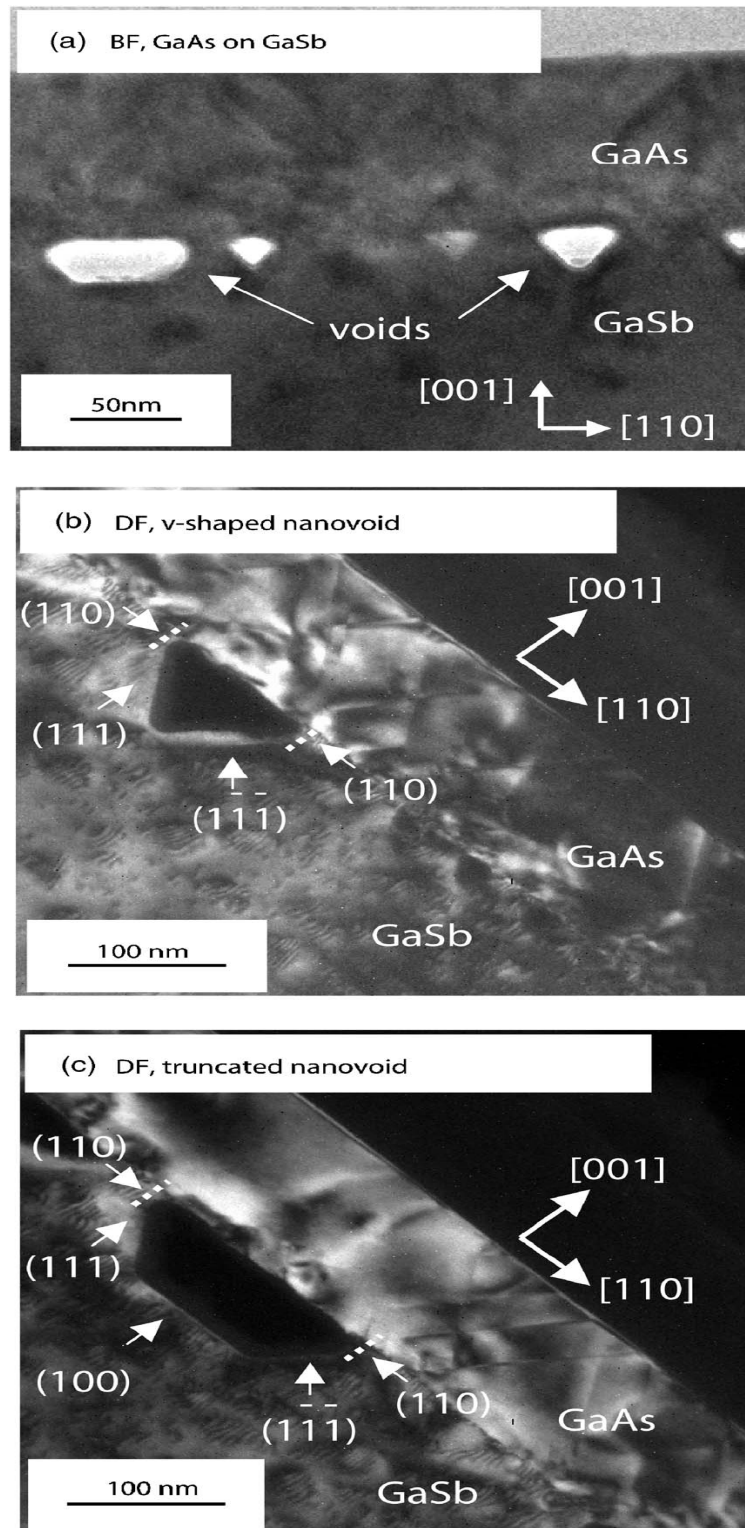
Figure 7. (a) Bright-Field XTEM Image of GaAs/GaSb Interface, Featuring Nanovoids, (b)DF XTEM (220) Image of GaAs/GaSb Interface, Showing a Single V-Shaped Nanovoid, (c) DF XTEM (220) Image of GaAs/GaSb Interface, Showing a Single Truncated V-Shaped Nanovoid

12

The etch rates of the GaAs/GaSb surface along certain crystallographic directions determine the formation of these facets. The typically observed hole width on the surface is $W \sim 50$ nm, while the height of the isosceles triangle is $t \sim 35$ nm. The dark field (DF) TEM images of the GaAs/GaSb surface shown in Figures 7(b) and 7(c) highlight the coalescence of GaAs over the nanovoids. There is a large lattice mismatch between the GaAs and GaSb layers. As a result, strain exists between these two layers. This strain is relaxed through defects, known as threading dislocations, as can be seen in Figure 7(b). The threading dislocation density is significant at the GaAs/GaSb interface as well as in the GaAs capping layer, over the voids. Figure 7(c) shows the DF image of a truncated nanovoid, and also, elucidates the GaAs coalescence over it. This truncated nanovoid is larger than the V-shaped nanovoid and seems to have a lower threading dislocation density. This is speculated to be because of the fact that the truncated nanovoids have a larger area of GaAs not in contact with GaSb, and therefore, they can relieve the strain occurring due to the mismatch more effectively, resulting in a lower defect density. The shape of etched nanovoids can be varied between an inverted triangle and a trapezoid by varying the substrate temperature during the etching. A higher temperature etching process of 570 ºC results in trapezoidal nanovoids.

The surrounding material of two different nanovoids is shown in the high-resolution TEM (HR-TEM) images of Figures 8(a) and 8(b). The thick coating on the {111} planes indicate the presence of amorphous material on the inside of the void. No TEM diffraction pattern was produced by the amorphous material. This amorphous material could either be excess Sb caused by the anion exchange reaction, shown in Equation (1), or the isoelectronic AsSb compound caused by the alternate reaction, given in Equation (2).

The etching rate in (111) planes is thought to decrease because of the amorphous elemental Sb or AsSb layer [11]. The accumulation of the surface AsSb or Sb on the side walls of nanovoids implies that the etching in the (110) direction occurs at a higher rate than along the (100) direction. This causes the pit to increase in width faster, compared to the rate of increase in depth. The result is a (100) plane at the bottom of the nanovoid, along with the formation of truncated V-shaped pits. Crystallographic adatom incorporation over the {111} planes appears to be prevented by this amorphous deposition. Eventually, the overgrowth of GaAs proceeds from the (110) planes and a coalescing occurs over the pit. While the overgrowth of the GaAs has been shown in Figure 6(b), the (110) nucleation site can be seen in the higher-resolution image, shown in Figure 8(a).

Figure 8(b) is an XTEM image, elucidating the nanovoid as seen through several atomic layers in front of the void. This image allows for only the crystalline material in front of the nanovoid to be seen, {111} planes are the terminating facets and the {110} planes are the planes on which the nucleation occurs. The difference in material thickness makes the nanovoids appear lighter in contrast to the surrounding material.
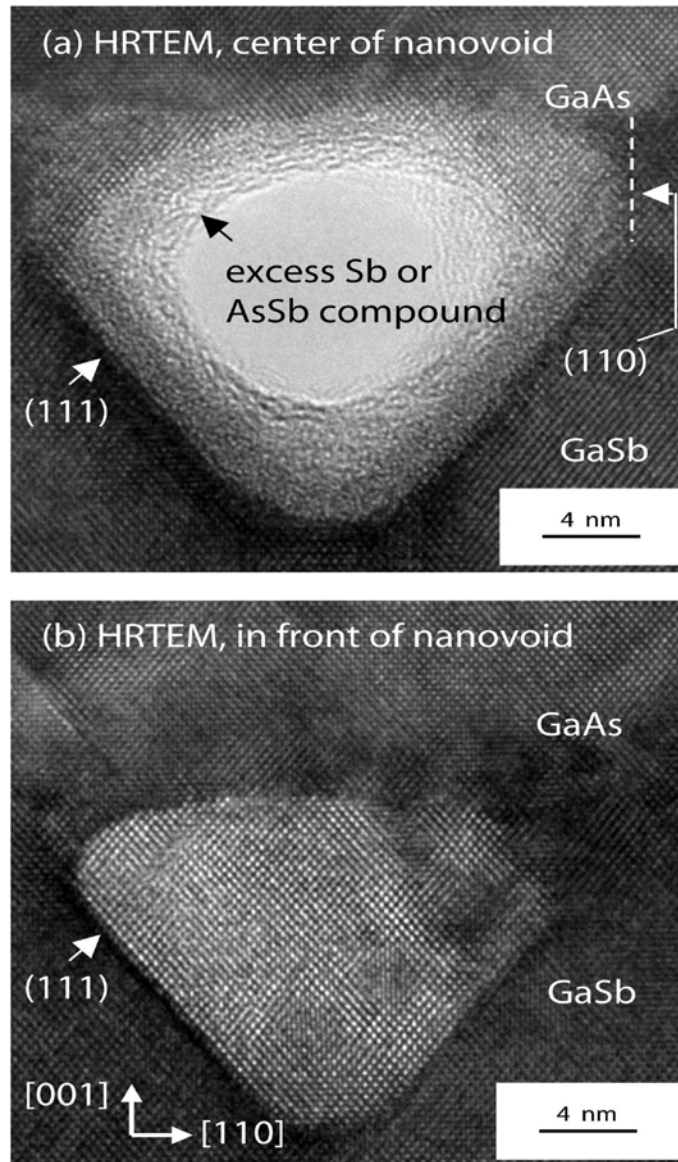
Figure 8. (a) HR-XTEM Image of a Single Nanovoid with Amorphous Coating, Figure, (b) HR-XTEM Image of a Nanovoid Viewed Through Several Atomic Layers, Showing Their Crystalline Structure

4.2. Testing of Temperature Sensitivity of CdSe/ZnS Core/Shell Quantum Dots

4.2.1. Etch Profile Analysis. An etch profile analysis of the wafer was carried out using an Alpha-Step profilometer. A typical result is shown in Figure 9.

According to the graph shown in Figure 9, the one-minute etch performed using 30% KOH solution resulted in a depth of 1 μm. This confirmed that we were able to carry out the etching successfully.

14
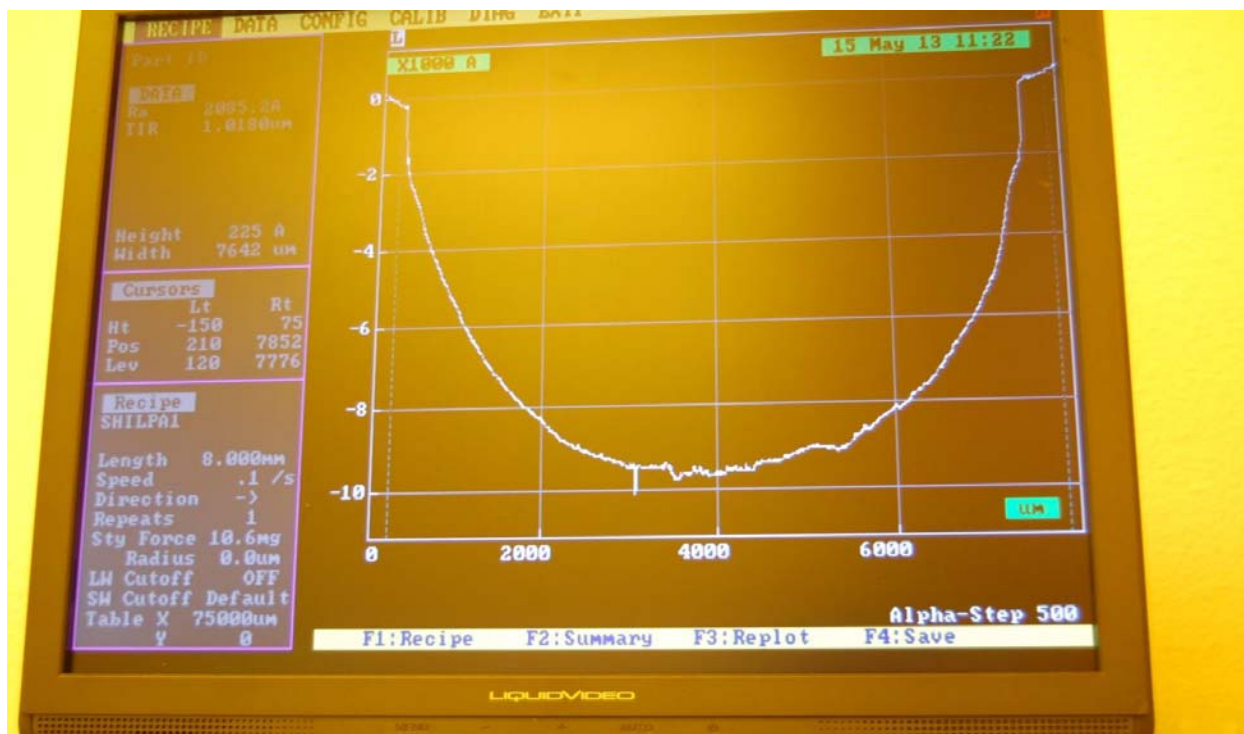
Figure 9. Etch-Profile of the Silicon Wafer Surface After a One-Minute KOH Etch

4.2.2. Calcination of the Quantum Dots. A depression created in the silicon wafer was then used to contain the CdSe/ZnS core/shell CQDs, placed there using a pipette. Calcination was then carried out to check if the QDs could withstand the high regrowth temperatures of around 700 °C inside the MBE chamber. A Si wafer containing the QDs was placed inside the oven and heated to 700 °C for 15 min.

PL and photoluminescence excitation (PLE) measurements on the QDs were done both before and after the heat treatment using a Horiba Jobin Yvon Fluorolog-3 spectrofluorometer, using a solid sample holder and front facet detection. As shown in Figure 10, the QDs exhibited strong fluorescence prior to the calcination process. Figure 10(a) shows an emission spectrum from the CdSe/ZnS core/shell QDs fixed on a Si wafer. Figure 10(b) shows an excitation spectrum from the CdSe/ZnS core/shell QDs fixed on a Si wafer. After calcination, no PL was observed. It is speculated that the organic coating around the QDs protected them from oxidation, and, upon calcination, the organic ligands were burned off, leaving behind bare QDs that were very susceptible to oxidation, a process which had detrimental effects on the PL of the sample.

15

(a)

(b)
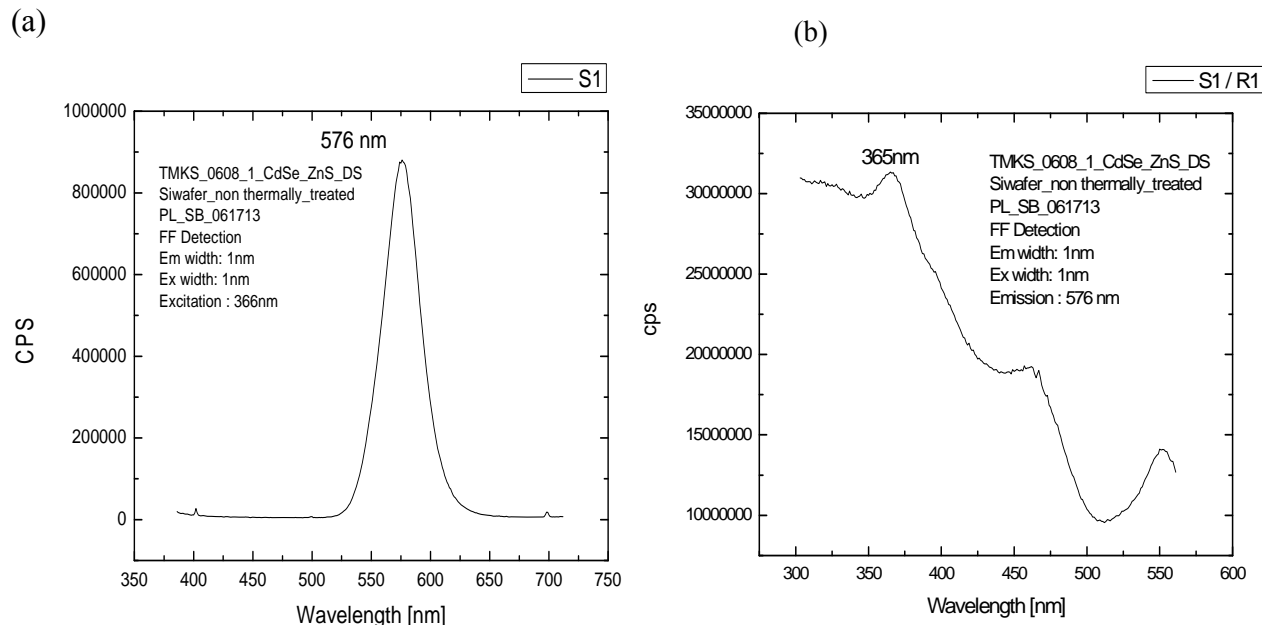
Figure 10. PL and PLE Measurements of CdSe/ZnS QDs Prior to the Calcination Process

4.2.3. Heat Treatment of the QDs in a Vacuum Environment. The rationale for heat treatment inside the MBE loading chamber was to simulate the environment that the QDs would be subjected to when the capping layer of GaAs was regrown over the exposed nanovoids containing the dots.

At first, a bare clean Si wafer, without the QDs, was placed inside the heating chamber of the MBE to check for any outgassing. The highest possible temperature that could be reached in this particular chamber was 480 °C (relatively close to the regrowth temperature). This particular chamber could be sealed off from the other growth chambers inside the MBE, thereby, posing no danger of contaminating the other chambers if significant outgassing occurred. It was observed that the wafer did not outgas at 480 °C. Next, the CdSe/ZnS QDs were placed into the depression created on the same Si wafer. This sample was then loaded into the same heating chamber of the MBE machine. The sample was heated to 480 °C for fifteen minutes and it was also made sure that no excessive amount of outgassing took place. The sample was, then, allowed to cool down and removed carefully from the MBE. PL measurements were done right after and compared with the PL measurements of the QDs observed prior to the heat treatment. The observations are shown in Figure 11.

Figures 11(a) and 11(b) show PL and excitation spectra, respectively, before the Si wafer containing the QDs was thermally treated. The CdSe/ZnS QDs were excited using a wavelength of 355 nm and an intensity of 1,000,000 counts per second (cps) was observed before the heat treatment. Figures 11(c) and (d) show PL and excitation spectra, respectively, after the Si wafer containing the QDs was thermally treated at 480 ºC inside the MBE loading chamber. The intensity dropped by about fifty times to 20,000 cps after the thermal treatment in the MBE. We

16

also observed that prior to the heat treatment the excitation peak occurred at 365 nm when checked for emission at 575 nm, while after the treatment the excitation peak was no longer high enough and other peaks (lamp artifacts) could also be seen.

(a)

(b)

(c)

(d)
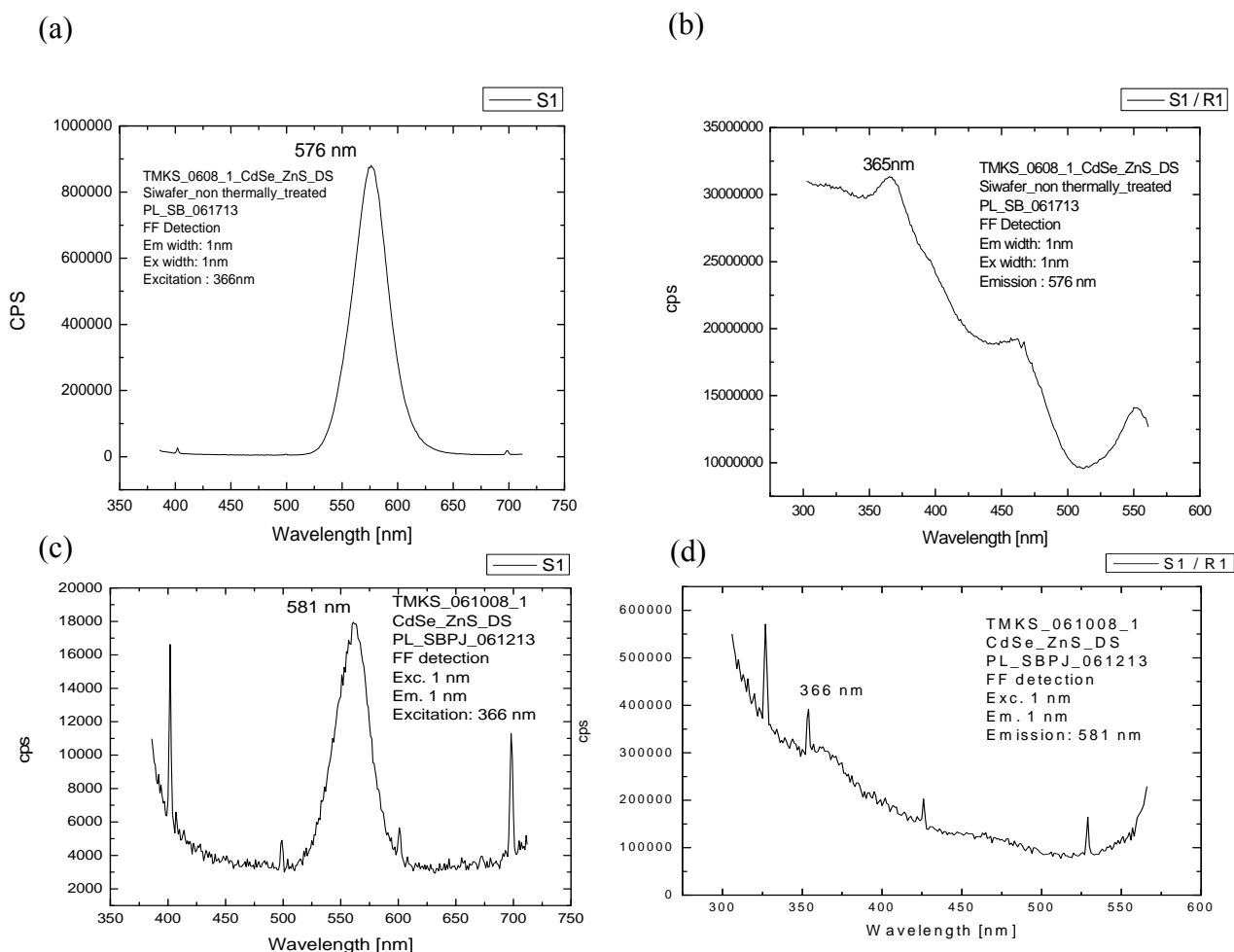
Figure 11. PL and PLE Spectra from CdSe/ZnS QDs Before and After Thermal Treatment at 480 ºC Under Vacuum

Further experiments were necessary to investigate whether the QDs retained their core-shell structure or any intermixing occurred between the two layers. This was done by annealing the QDs in a vacuum environment at different temperatures starting from 200 °C, and measuring the PL and quantum efficiency (QE) to observe any shifts in the PL spectra.

The QDs were placed on a 1×1 cm^2 sapphire substrate (Fig. 12). Sapphire was chosen as it is highly transparent to wavelengths of light between 150 nm (UV) and 5500 nm (infrared), and as such, it would not interfere with the PL from the QDs. PL of the bare sapphire substrate was measured to verify that there was no emission from the 362 nm excitation wavelength of the QDs. Next, 1.0 μL of the QDs were pipetted onto the center of the sapphire substrate. Figure 12 shows emission around 570 nm under a UV lamp illumination.

17
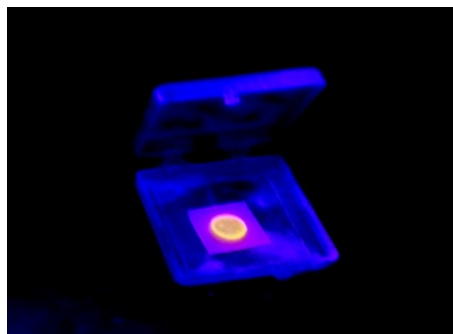
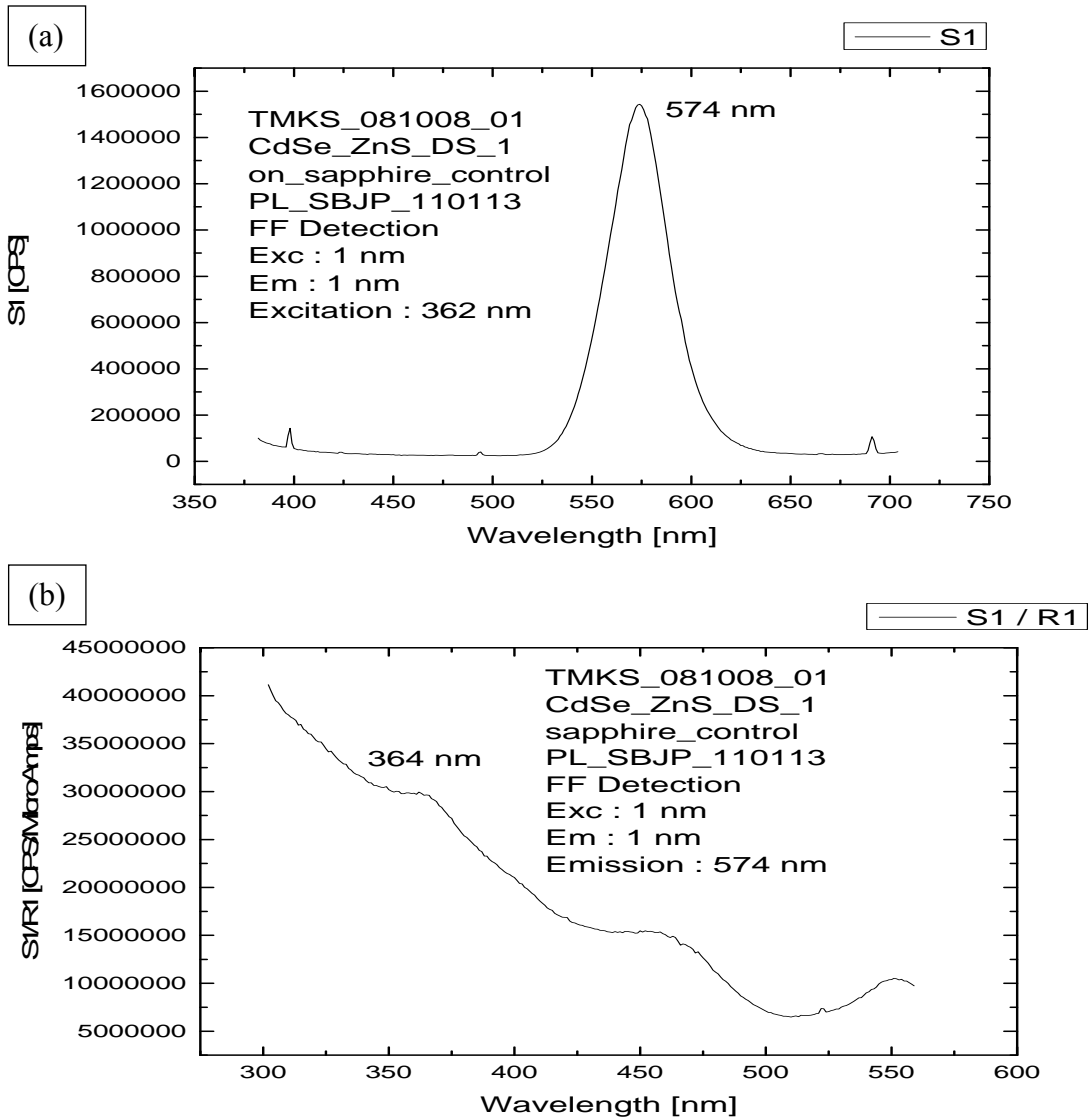**Figure 12. CdSe/ZnS Core/Shell QDs on a Sapphire Holder**

The PL at room temperature was measured, at first, to serve as a control for comparison with the PL obtained at each of the higher temperatures. The QD annealing experiments were carried out in the preparation chamber of the MBE system in a vacuum environment by heating them to 200 °C and increasing the temperature at steps of 50 °C until the QDs stopped exhibiting any PL, which occurred at 250 °C. The PL and QE were measured at each of these temperatures as shown in Figures 13, 14, and 15. QE measurements were performed using the Fluorolog-3 integrating sphere attachment and a solid sample holder.

Figure 13 shows the PL and PLE spectra from the CdSe/ZnS QDs on sapphire measured at room temperature. The PL spectra in Figures 13(a) and 13(b) show that at room temperature the CdSe/ZnS QDs on sapphire emitted strongly at 574 nm, with a 1.40 million cps, for an excitation wavelength of 362 nm. When measuring the PLE using a 574 nm parked emission wavelength, the excitation spectrum increases in intensity well into the UV, as shown in Figure 13(b). However, because the walls of the integrating sphere, which was used to measure the QE, start absorbing light at around 360 nm, the 362 feature on the PLE spectrum was chosen as the standard excitation wavelength.
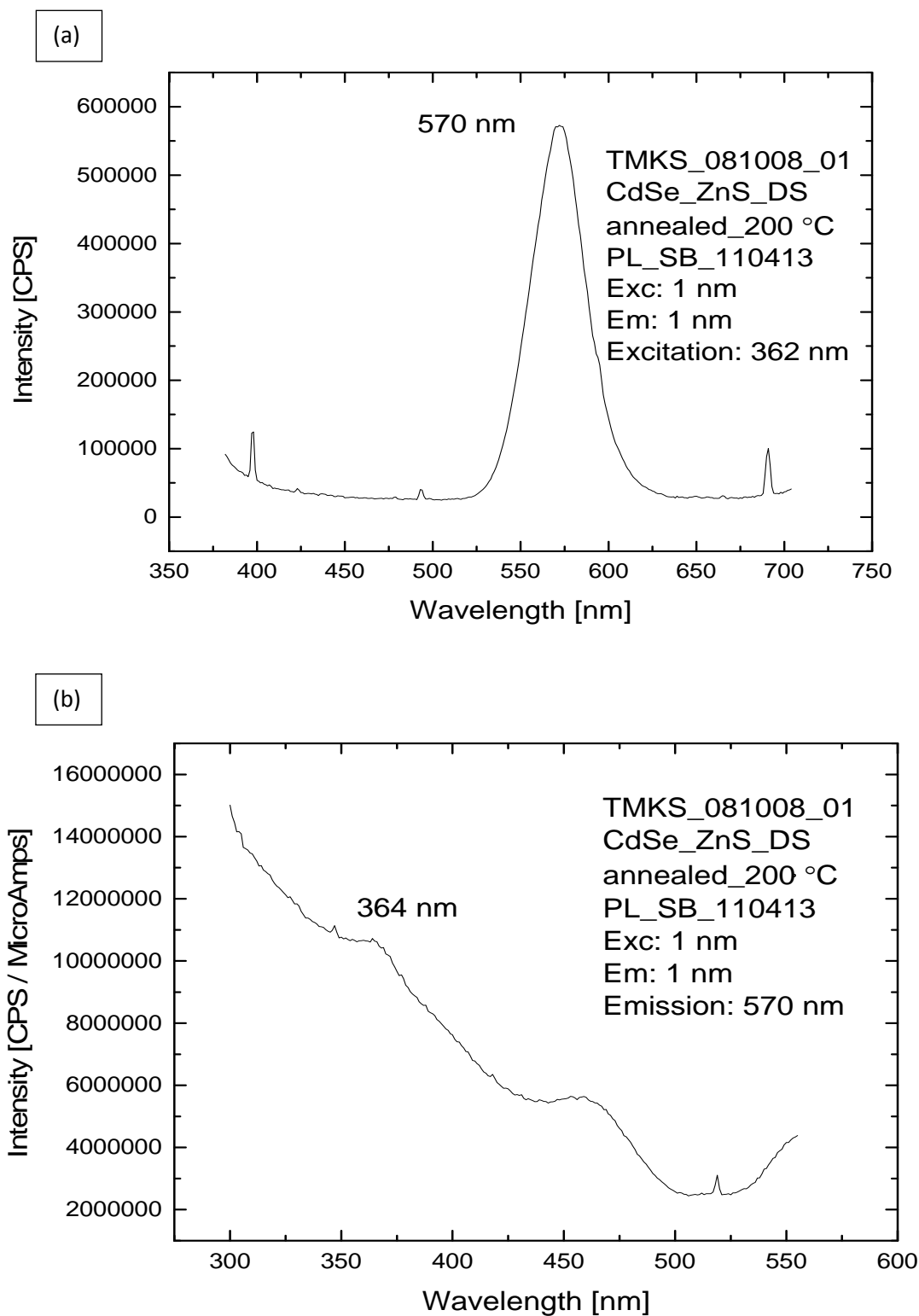
The PL and PLE spectra of the QDs annealed at 200 °C in a vacuum environment inside the MBE system are shown in Figures 14(a) and 14(b), respectively. An emission peak at 570 nm was observed, for a 362 nm excitation. The intensity of the QDs decreased by 2.5 times to 0.56 million cps at this temperature. When checked for the 570 nm emission, a PLE feature at 364 nm wavelength was observed, indicating no significant shift in the PL spectra.

The PL and PLE spectra of the QDs annealed at 250 °C in a vacuum environment inside the MBE system are shown in Figures 15(a) and 15(b), respectively. The emission peak and excitation feature remained at 573 nm and 364 nm, respectively, indicating that there was no shift in the spectra. The emission intensity, however, dropped by about 7 times to only 0.2 million cps this time.

The QE at room temperature was measured to be very high at 95.8%. It decreased to about 30% when the QDs were annealed at 200 °C. Finally, after annealing at 250 °C, the QE dropped to about 4%. From these results, we concluded that the CdSe/ZnS QDs lost their PL emission at temperatures of 250 °C and above.

Figure 13. PL (a) and PLE (b) Spectra of CdSe/ZnS QDs on Sapphire at Room Temperature

(a)

600000

500000

400000

Intensity [CPS]

300000

200000

100000

0

570 nm

TMKS_081008_01
CdSe_ZnS_DS
annealed_200 °C
PL_SB_110413
Exc: 1 nm
Em: 1 nm
Excitation: 362 nm

350   400   450   500   550   600   650   700   750

Wavelength [nm]

(b)

16000000

14000000

12000000

Intensity [CPS / MicroAmps]

10000000

8000000

6000000

4000000

2000000

364 nm

TMKS_081008_01
CdSe_ZnS_DS
annealed_200 °C
PL_SB_110413
Exc: 1 nm
Em: 1 nm
Emission: 570 nm

300   350   400   450   500   550   600

Wavelength [nm]

Figure 14. PL (a) and PLE (b) Spectra of CdSe/ZnS QDs on Sapphire Annealed at 200 °C in Vacuum

20
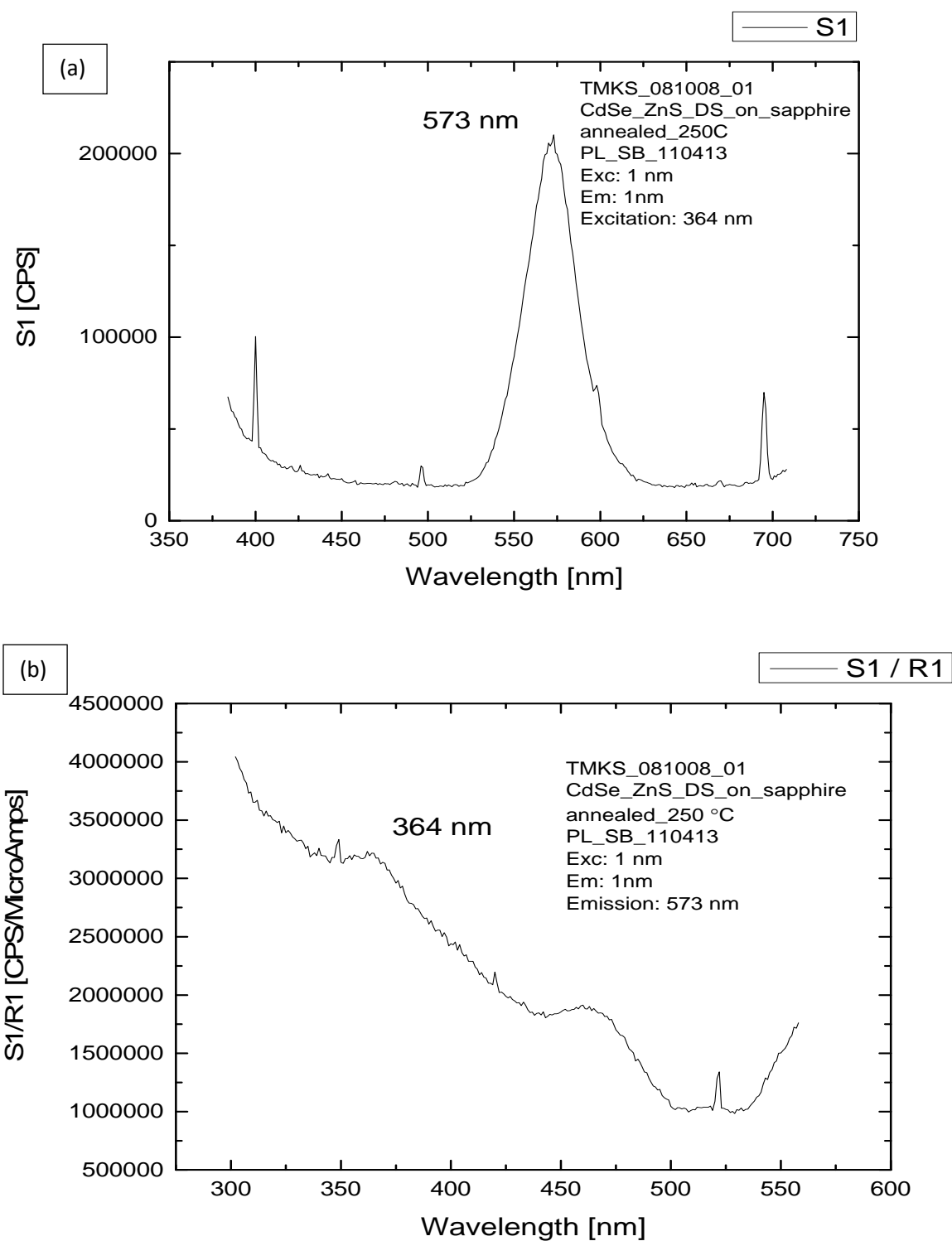
Figure 15. PL (a) and PLE (b) Spectra of CdSe/ZnS QDs on Sapphire Annealed at 250 °C in Vacuum

21

4.3   PL Spectra of Quantum Dots in Nanovoids

1.0 µL of the CdSe/ZnS CQDs were pipetted onto the nanovoid GaAs/GaSb sample. The sample was etched for 5 min to selectively etch off the coalescing GaAs capping layer and expose the GaSb nanovoids. PL measurements were performed on this sample before and after placing the QDs. The PL measured on a sample without the QDs (Fig. 16) served as a control. It was done to show that there was no emission from the bare GaAs/GaSb nanovoid sample when excited at 364 nm, which is the excitation wavelength for the QDs, as mentioned previously.
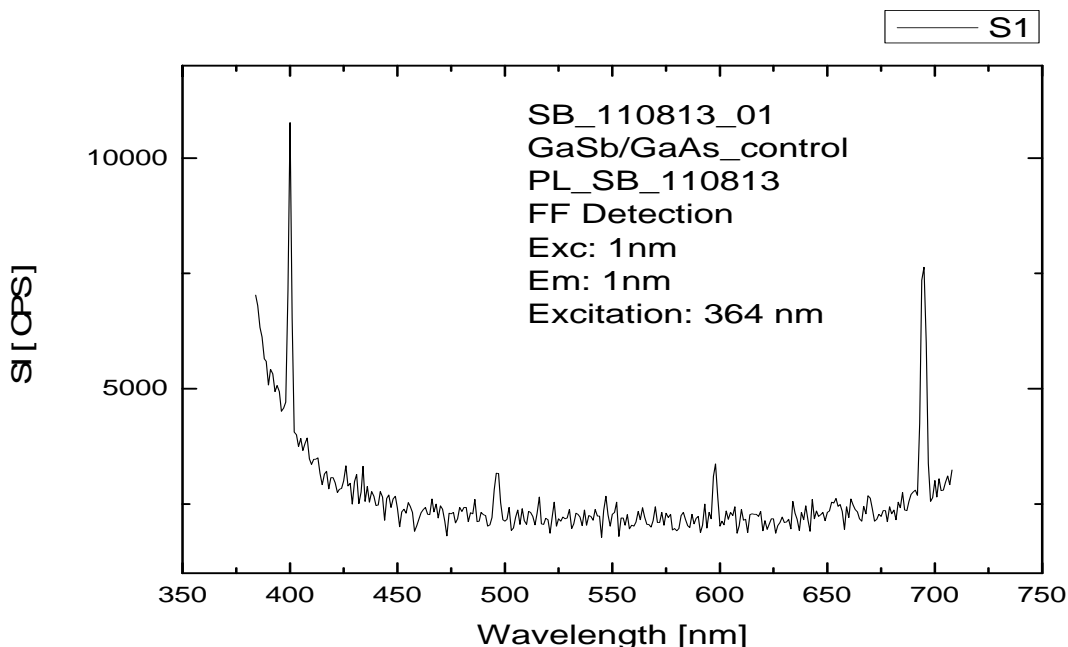

**Figure 16. PL Spectrum of a Bare GaAs/GaSb Nanovoid Sample**

The PL and PLE spectra of the CdSe/ZnS QDs placed on a GaAs/GaSb nanovoid sample are shown in Figures 17(a) and 17(b), respectively. The emission peak and excitation feature were observed at 574 nm and 364 nm respectively, as expected. A strong emission intensity of 2.5 million cps was observed. This indicated that the colloidal QDs were able to fluoresce when placed on the nanovoid sample. However, a QE of only 5.3% was observed, as opposed to a QE of 95.8% when the CQDs were placed on sapphire. This is due to the fact that the bandgap of GaAs is too low, and because of it, GaAs absorbed the excitation wavelength of the QDs to reduce the apparent QE. Sapphire, on the other hand, has a wide optical transmission band (from UV to near infrared), making it highly transparent to the excitation wavelength of the QDs and thereby, resulting in a higher QE.

22

4.4   Electron Microscopy of Quantum Dots in Nanovoids

The QDs placed on an etched GaAs/GaSb nanovoid sample (R12-128) were examined by electron microscopy. XTEM of the sample was done to check for the integration of the CdSe/ZnS QDs with the GaSb nanovoids (Figs. 18-20). QDs were observed to occupy the space above the sample surface as well as inside the nanovoids.
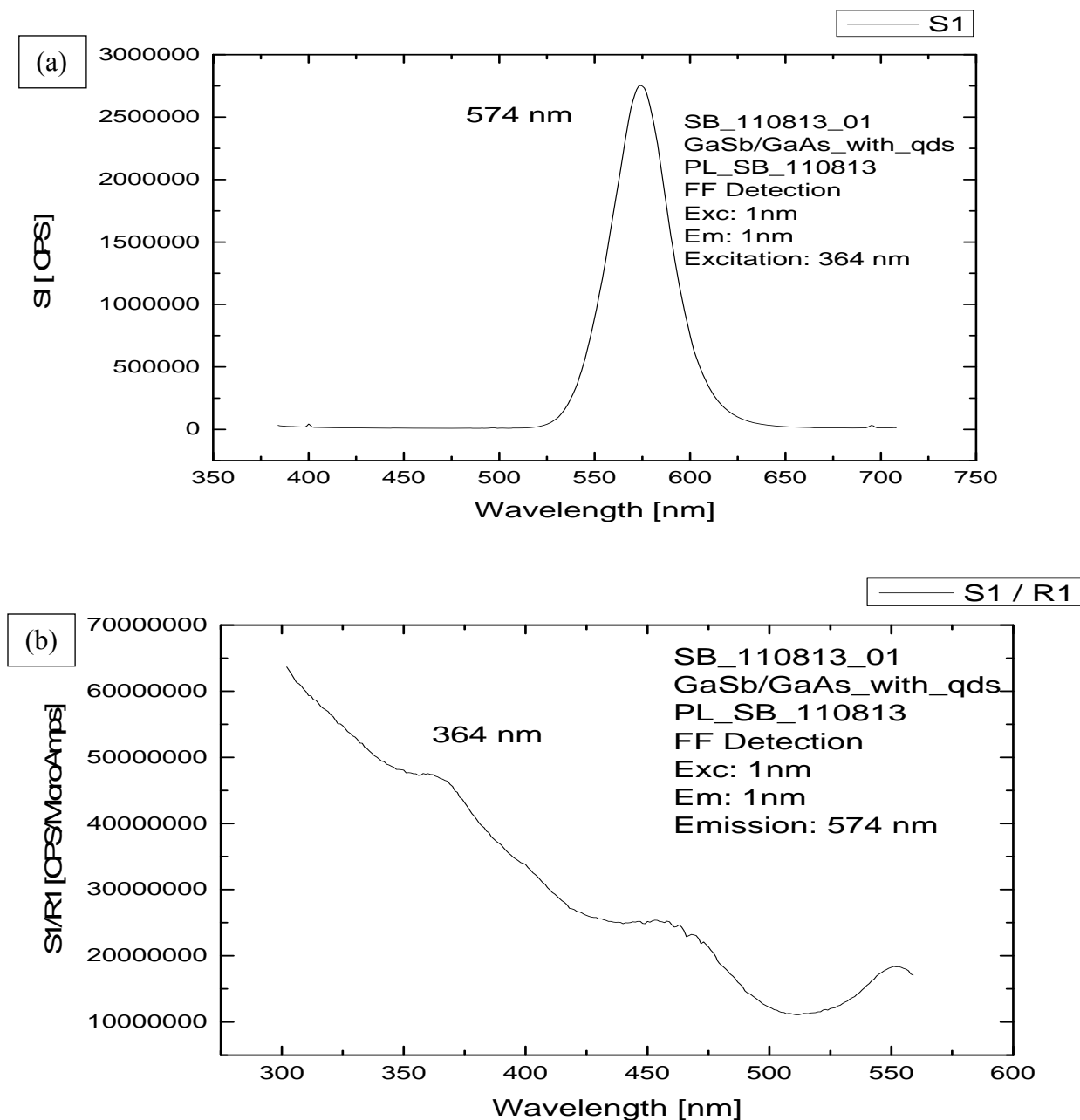
Figure 17. PL (a) and PLE (b) Spectra of CdSe/ZnS QDs Placed on a GaAs/GaSb Nanovoid Sample

Approved for public release; distribution is unlimited.
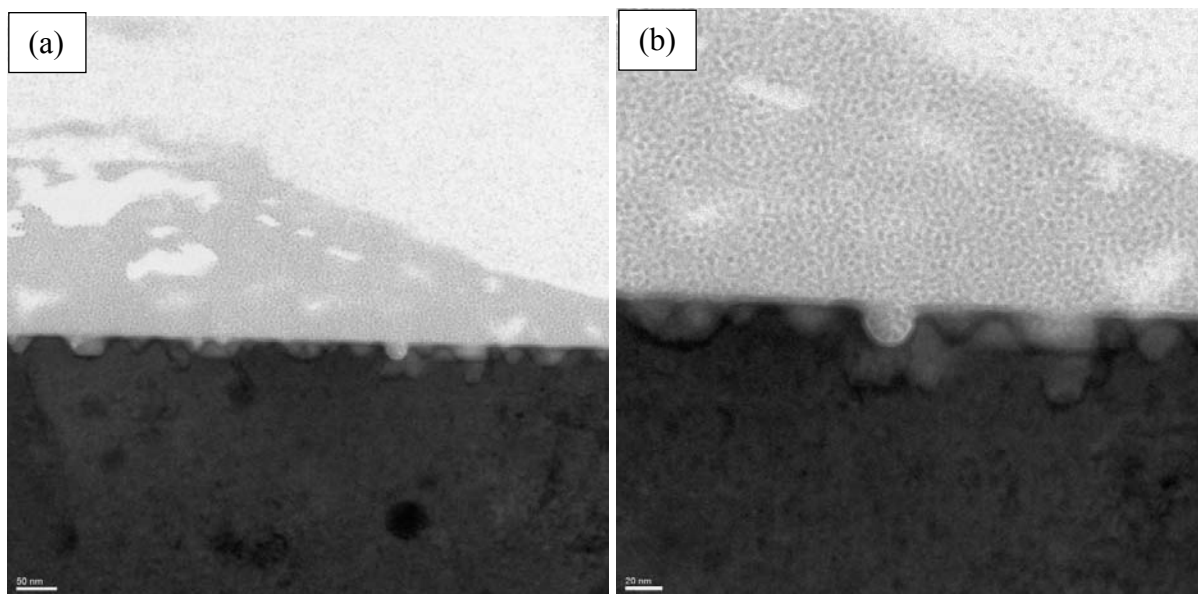
Figure 18. XTEM Images of CdSe/ZnS QDs on a GaAs/GaSb Nanovoid Sample. Scale Bars 50 nm (a) and 20 nm (b)
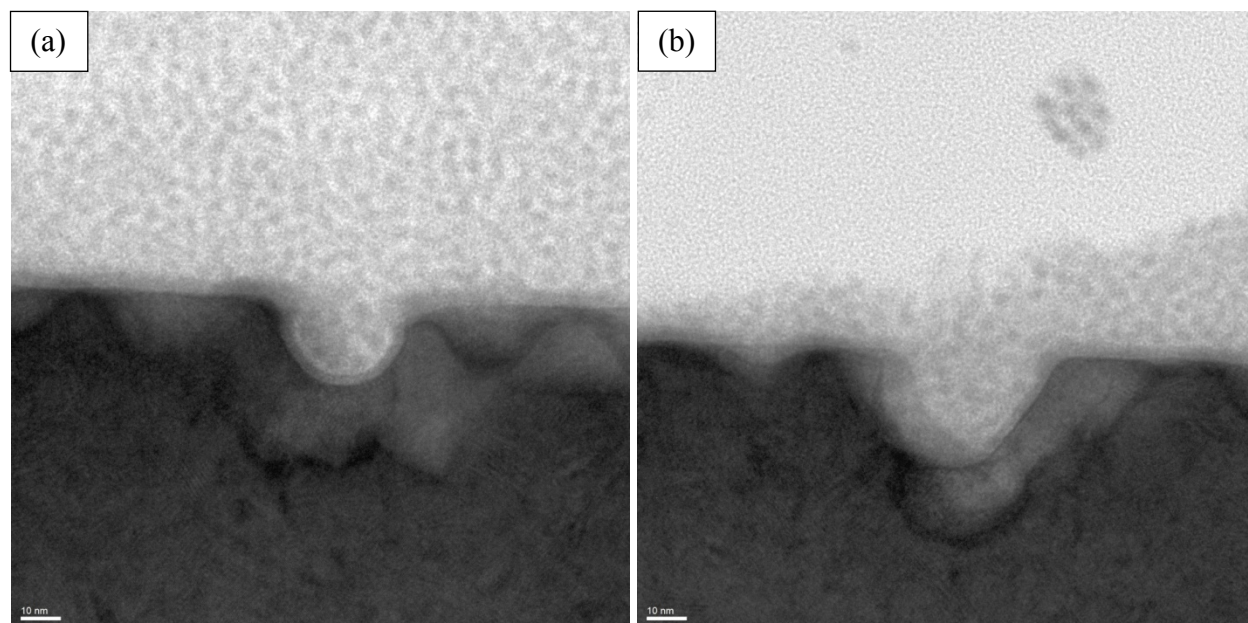
Figure 19. XTEM Images of the QDs on the GaAs/GaSb Nanovoid Sample at a Higher Resolution (Scale Bar 10 nm)

A line energy-dispersive X-ray spectroscopy (EDS) was also performed on the sample (Fig. 21). EDS makes use of the X-ray spectrum emitted by a solid sample bombarded with a focused beam of electrons to obtain a localized chemical analysis. Figure 21(a) shows a TEM image

24

indicating the regions on which EDS measurements were performed. Figure 21(b) shows the EDS spectrum for region 1, with clear peaks of Cd, Se, Zn, and S proving the gray region to contain the QDs. Figure 21(c) shows the EDS of region 2 with a strong C peak, indicating that the dark regions contain carbon. Figures 21(d) and (e) show the EDS spectra of regions 3 and 4, respectively, with the peaks of Cd, Se, Zn, and S indicating the presence of QDs on the sample surface. These results confirm that the small gray objects in the images of Figures 18-20 are the QDs, and that the QDs have entered the nanovoids. A lot of carbon resulting from the QD capping and from the organic solvent in which the QDs were suspended can be seen on the surface. This could be eliminated by calcinating the QDs before depositing them on the GaSb surface. A capping layer can, next, be grown over the nanovoids to enclose the QDs in them.
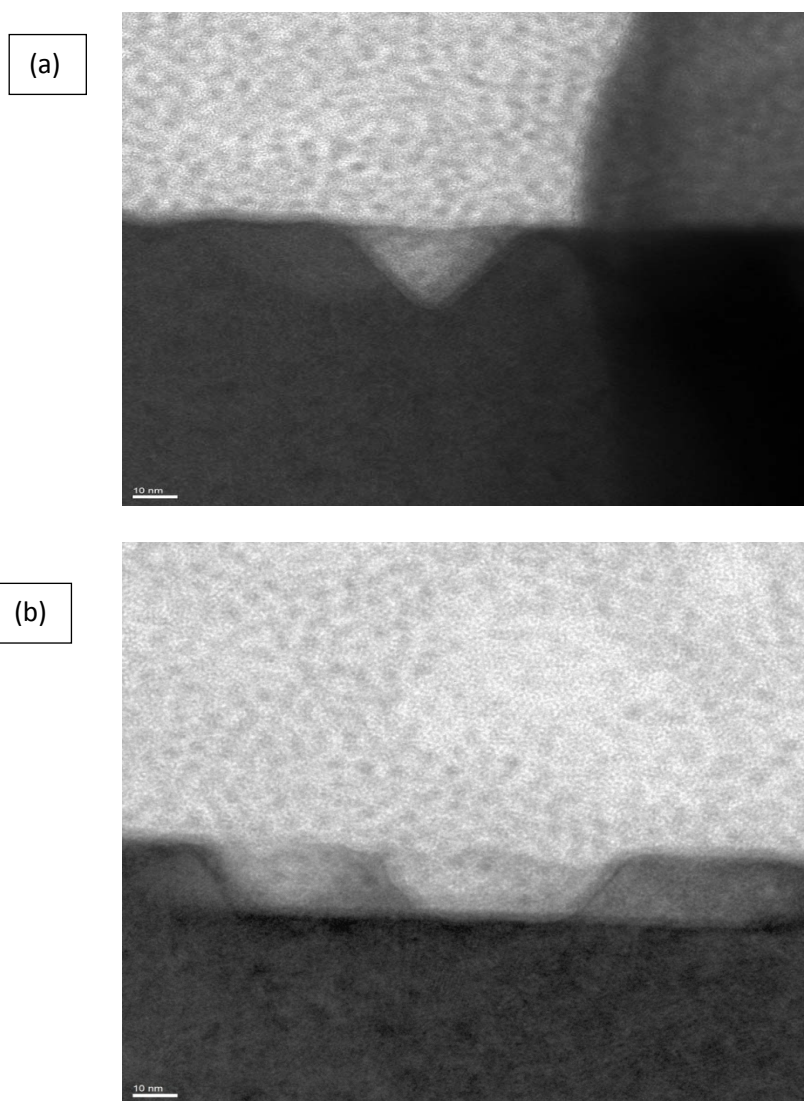
Figure 20. XTEM Images of Other Regions of the GaAs/GaSb Nanovoid Sample
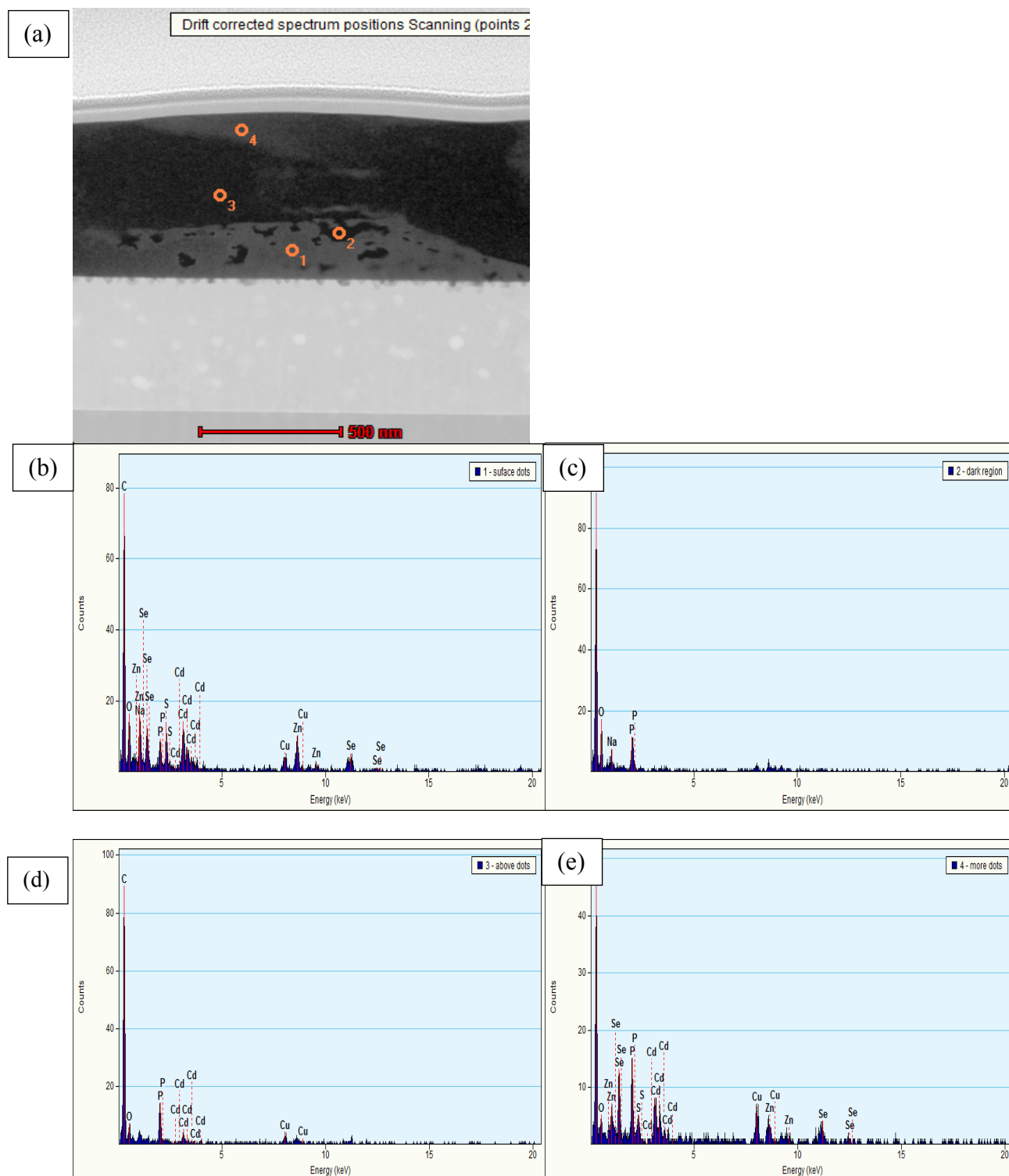
Figure 21. EDS Study of CdSe/ZnS QDs on the Surface of GaAs/GaSb Nanovoid Sample

5.0   CONCLUSIONS

QDs due to their small size portray unique optical properties that are different compared to those of the bulk material. The most apparent of these properties is the excitation of the dots resulting in emission of photons, which are visible to the human eye as light. More interestingly, the wavelength of these photon emissions does not solely depend on the type of material from which the QDs are made; but, in addition, it depends on the size of the QDs. The QDs can also be tuned accordingly to emit into the UV or into the infrared.

In this report, we first describe the *in-situ* nanoscale etch-pit formation on GaSb (100) surfaces as a result of exposure to As_2 in the molecular beam epitaxy. The impinging As_2 atoms cause a Sb-displacement on the GaSb substrate, resulting in the formation of the pits. The dimensions of these nanopits increase with As_2 exposure time. Subsequent growth of GaAs over these nanopits proceeds by a coalescence mechanism, resulting in highly faceted interfacial nanovoids. TEM image of the nanoscale pits showed that they are highly faceted and that a layer of amorphous material (excess As_2 or AsSb) terminated the facets.

The key objective of this project was to embed QDs into the nanovoids. In order to do this, experiments and measurements were carried out initially to check the ability of the QDs to fluoresce in the high regrowth temperatures inside the molecular beam epitaxy. CdSe/ZnS QDs were used, considering their high QE and high stability over time. The procedure for the synthesis of the colloidal CdSe/ZnS core/shell QDs was summarized. Silicon wafers were checked for outgassing and then used to contain the QDs to carry out the optical measurements. Experimental procedures, PL and QE measurements of the QDs on silicon and sapphire substrates subjected to different temperatures in a vacuum environment were described to conclude that the QDs lost their PL at temperatures of 250 °C and above. This indicated that a capping layer of GaAs would not be possible for the nanovoids when the CdSe/ZnS QDs are in it, as GaAs had regrowth temperatures above 500 °C. Moreover, GaAs having a low bandgap would absorb any emission from the QDs. An alternate capping layer could be silicon dioxide, owing to its lower deposition temperature and wider bandgap. Finally, the QDs were placed on the GaAs/GaSb nanovoid sample and were seen to, still, emit strongly on this surface. Integrating the CdSe/ZnS QDs into these nanovoids was successful, as confirmed by TEM and EDS data. This indicated a successful demonstration of integration of dissimilar compounds (III-V and II-VI). The ability to successfully place the QDs into the nanovoids can pave way to useful technological applications for the optoelectronics industry.

REFERENCES

[1] M. H. Baier, S. Watanabe, E. Pelucchi, and E. Kapon, "High uniformity of site-controlled pyramidal quantum dots grown on prepatterned substrates," *Appl. Phys. Lett*. **84** (#11), pp. 1943-1945, 2004.

[2] S. H. Huang, G. Balakrishnan, M. Mehta, L. R. Dawson, D. L. Huffaker, and P. Li, "Arsenic-induced etched nanovoids on GaSb (100)," *J. Appl. Phys*. **102,** Art. 044312, 2007.

[3] M. Losurdo, P. Capezzuto, G. Bruno, A. S. Brown, T. Brown, and G. May, "Fundamental reactions controlling anion exchange during mixed anion heterojunction formation: Chemistry of As-for-Sb and Sb-for-As exchange reactions," *J. Appl. Phys*. **100** (#1), Art. 013531, 2006.

[4] D. E. Ibbotson, D. L. Flamm, and V. M. Donnelly, "Crystallographic etching of GaAs with bromine and chlorine plasmas," *J. Appl. Phys*. **54** (#10), pp. 5974-5981, 1983.

[5] J. Berger and D. Fekete, "Monolithic integration of AlGaAs/GaAs laser and external mirrors," *J. Electrochem. Soc*. **46** (#9), pp. 806-808, 1985.

[6] P. D. Brewer, D. McClure, and R. M. Osgood, "Dry, laser-assisted rapid HBr etching of GaAs," *Appl. Phys. Lett*. **47** (#3), pp. 310-312, 1985.

[7] A. R. Clapp, E. R. Goldman, and H. Mattoussi, "Capping of CdSe–ZnS quantum dots with DHLA and subsequent conjugation with proteins," *Nature Protocols* **1** (#3), pp. 1258-1266, 2006.

[8] M. M. Ul Islam, "Difference between silicon wafer <100> & <111>," http://www.academia.edu/334549/Difference_between_silicon_wafer_100_and_111_. Accessed April 21, 2013.

[9] H. Seidel, L. Cseprege, A. Heuberger, and H. Baumgarel, "Anisotropic etching of crystalline silicon in alkaline solutions," *J. Electrochem. Soc.* **137** (#11), pp. 3612-3626, 1990.

[10] University of California Irvine, "Wet anisotropic Si etch using KOH," INRF Application Note, http://www.inrf.uci.edu/wordpress/wp-content/uploads/sop-wet-anisotropic-si-etch-using-koh.pdf . Accessed May 15, 2013.

[11] C. L. Lin, Y. K. Su, T. S. Se, and W. L. Li, "Variety transformation of compound at GaSb surface under sulfur passivation," *J. Appl. Phys., Pt 2* **37**, pp. L1543-L1545, 1998.

List of Symbols, Abbreviations, and Acronyms

AFM – atomic-force microscope
Ar – argon
As – arsenic
BEP – beam equivalent pressure
BF – bright field
Cd – cadmium
$Cd(acac)_2$ – cadmium acetylacetonate
CdSe – cadmium selenide
cm – centimeter
cps – counts per second
CQD – colloidal quantum dot
DI – de-ionized
EDS – energy-dispersive spectroscopy (EDS)
g – gram
GaAs – gallium arsenide
GaSb – gallium antimonide
HDA – hexadecylamine
HDD – hexadecanediol
HR-SEM – high-resolution scanning electron microscope
HR-TEM – high-resolution transmission electron microscope
IPA – isopropyl alcohol
kJ – kilojoule
KOH – potassium hydroxide
kV – kilovolt
M – molar
MBE – molecular-beam-epitaxy
mg - milligram
mL – milliliter
ML – monolayer
nm – nanometer
PL – photoluminescence
PLE – photoluminescence excitation
QD – quantum dot
QE – quantum efficiency
RHEED – reflective high-energy electron beam
Sb – antimony
Se – selenium
SEM – scanning electron microscope
Si – silicon
TEM – transmission electron microscopy
$(TMS)_2S$ – bis(trimethylsilyl) sulfide
TOP – trioctyl phosphine
TOPO – trioctyl phosphine oxide

TOPSe – trioctyl phosphine selenide
UV – ultraviolet
XTEM – cross-sectional transmission electron microscopy
$ZnEt_2$ – diethylzinc
ZnS – zinc sulfide
μL – microliter
μm – micrometer

DISTRIBUTION LIST

DTIC/OCP
8725 John J. Kingman Rd, Suite 0944
Ft Belvoir, VA 22060-6218   1 cy

AFRL/RVIL
Kirtland AFB, NM 87117-5776   2 cys

Official Record Copy
AFRL/RVSE/Clay Mayberry   1 cy

(This page intentionally left blank)